Evolution of microscopic and mesoscopic synchronized patterns in complex networks

Jesús Gómez-Gardeñes,[1,2,a)] Yamir Moreno,[2,3] and Alex Arenas[2,4]

[1]*Departamento de Física de la Materia Condensada, Universidad de Zaragoza, 50009 Zaragoza, Spain*
[2]*Institute for Biocomputation and Physics of Complex Systems (BIFI), University of Zaragoza, Zaragoza 50018, Spain*
[3]*Departamento de Física Teórica, Facultad de Ciencias, Universidad de Zaragoza, Zaragoza 50009, Spain*
[4]*Departament d'Enginyeria Informàtica i Matemàtiques, Universitat Rovira i Virgili, Tarragona 43007, Spain*

Previous studies about synchronization of Kuramoto oscillators in complex networks have shown how local patterns of synchronization emerge differently in homogeneous and heterogeneous topologies. The main difference between the paths to synchronization in both topologies is rooted in the growth of the largest connected component of synchronized nodes when increasing the coupling between the oscillators. Nevertheless, a recent study focusing on this same phenomenon has claimed the contrary, stating that the statistical distribution of synchronized clusters for both types of networks is similar. Here we provide extensive numerical evidences that confirm the original claims, namely, that the microscopic and mesoscopic dynamics of the synchronized patterns indeed follow different routes. © *2011 American Institute of Physics*. [doi:10.1063/1.3532801]

Synchronization is at the core of diverse collective phenomena spanning a variety of life scales from social to neurological contexts.[1–3] On the other hand, most of the natural and social systems in which synchronization shows up have intricate connectivity patterns between their units that are nowadays described as complex networks.[4–7] Consequently, the question about how synchronization is affected by the architecture of such complex networks has spurred on a number of studies during the last decade.[8] In previous studies,[9,10] we showed that local patterns of synchronization evolve toward the fully synchronized state differently in homogeneous and heterogeneous complex networks for the case of Kuramoto oscillators. Namely, the transition to synchronization in homogeneous networks occurs when several synchronized clusters of similar (small) sizes collapse into one macroscopic cluster. In contrast, in scale-free heterogeneous networks, this transition is ruled by the hubs and takes place smoothly and centralized around the cluster that contains the hubs. Recently, the previous results have been challenged by a new study that focused on the same system[11] but using coarse grained data and statistical metrics (rather than nonaveraged quantities). Here we provide extensive numerical evidences that confirm our previous claims, namely, that the microscopic dynamics of the synchronized patterns indeed follow different routes.

I. INTRODUCTION

Synchronization is an emergent phenomenon found in natural and social networked systems, ranging from biological clocks to stock market crashes. Understanding synchronization processes in networks thus help advancing on the physical description of such different complex systems. Several studies have focused on this subject during the last few years, and as a result, we already understood some aspects about synchronization in networks.[8] Features that have been analyzed in depth include the formation and growth of synchronized clusters in networks before complete synchronization is attained and the study of the conditions needed for the onset of synchronization. The latter is particularly important to address the question of which topology is optimal for synchronization purposes, as far as it is intended as the ability of the system to form the first synchronized clusters. In fact, the ubiquity of scale-free networks in natural, social, and technological systems has given rise to a number of studies about the onset of synchronization on this type of topology,[9,10,12–19] which is characterized by large fluctuations in the number of connections a node may have. In addition, the same issue has also been studied on other (scale-free or not) network topologies with additional structural properties, such as gradient networks,[20] random geometric graphs,[25] clustered[22,23] and modular networks,[14,24] or weighted graphs.[26] These theoretical studies have paved the way toward a better understanding of complex synchronization patterns found in natural systems. This is the case of the onset of synchronization during both epileptic seizures[27] and neural development,[28] or the dynamical organization of the brain cortex.[29,30]

In recent works,[9,10] we compared how local patterns of synchronization emerge differently in homogeneous and heterogeneous scale-free complex networks. To this end, we implemented the Kuramoto model of coupled phase oscillators[31–33] on top of Erdös–Rényi (ER) and Barabàsi–Albert (BA) scale-free (SF) networks generated using a configurational model introduced in Ref. 34. In these works, we

a)Electronic mail: gardenes@gmail.com.

showed that the main difference between these topologies relies on the growth of the largest connected component of synchronized nodes when increasing the coupling between them. Nevertheless, these works showed these differences in terms of average values of the relevant physical quantities and thus constituted an indirect evidence of the differences between the two microscopic scenarios. The above numerical evidences have been distrusted recently by Kim *et al.*[11] who claimed that the difference in the microscopic evolution of synchronized patterns in ER and SF networks does not exist. In particular, by using a debatable scaling *ansatz* borrowed from percolation theory and finite size scaling to estimate the proposed scaling laws, they compute numerically the critical exponents, which turned to be practically the same in ER and SF networks.

In this work, we present the evolution of the synchronized clusters in terms of the statistical distributions of their descriptors together with the corresponding raw data as obtained from extensive numerical simulations. This new description allows to confirm our previous claims, namely, that the microscopic dynamics of the synchronized patterns follow different routes in homogeneous and heterogeneous networks. Therefore, we will not discuss the weaknesses of the asymptotic approach adopted in Ref. 11, instead we will offer clear numerical evidences that show that our previous claim was correct, and consequently that their theory should be revised.

II. THE MODEL

In order to explore computationally the evolution of synchronization patterns in degree-homogeneous and degree-heterogeneous complex networks, we consider networks of N nonidentical phase oscillators evolving according to the Kuramoto model[31]

$$\frac{d\theta_i}{dt} = \omega_i + \lambda \sum_{j=1}^{N} A_{ij} \sin(\theta_j - \theta_i) \quad i = 1, \ldots, N, \quad (1)$$

where ω_i stands for the natural frequency of oscillator i, λ is the coupling strength, and A_{ij} is the connectivity matrix of the network (defined as $A_{ij} = 1$ if i is linked to j and $A_{ij} = 0$ otherwise). It is well-known that the collective dynamics of coupled Kuramoto oscillators[32,33] undergoes a transition from incoherent dynamics to a synchronized regime as λ increases. The synchronization transition can be monitored by means of an order parameter r defined as

$$re^{i\Phi} = \frac{1}{N} \sum_{j=1}^{N} e^{i\theta_j}. \quad (2)$$

The value of r changes from $r \approx 0$ to $r \approx 1$ as the system goes from the incoherent state (at low values of λ) to the fully synchronized one (for large enough λ).

When the network of interactions, encoded in the adjacency matrix A_{ij}, has a nontrivial underlying structure, as it is the case for ER and SF graphs, it is interesting to analyze the synchronization transition by looking at the emergence of small clusters of synchronized nodes. In particular, we

focus on the evolution of these synchronized clusters that can be seen as small subgraphs embedded into the network along the whole synchronization transition. To this end, one starts at moderate coupling values to observe how certain parts of the system become synchronized rather fast whereas other regions still behave incoherently. Increasing the coupling strength, one monitors the synchronized patterns by reconstructing the subgraphs composed of those nodes and links that share the largest degree of synchronization. The study of the structural properties of these subgraphs can thus be performed accurately as the coupling λ is increased, allowing the characterization of those sets of nodes that drive the global dynamics of the system.

The numerical experiment designed to prove the difference between ER and SF networks with respect to the microscopic evolution of synchronized patterns is the following: we analyze 10^4 different realizations of the dynamics on both graphs, and every realization corresponds to a network made up of 10^3 oscillators with average degree $\langle k \rangle = 6$. For each realization, we set up a different initial condition by assigning to each oscillator an initial phase, $\theta_i \in [-\pi, \pi]$, and an internal frequency, $\omega_i \in [-1/2, 1/2]$, using uniform distributions in both cases. We integrate the system of equations (1) by means of a fourth order Runge-Kutta method with a time step of $\Delta t = 0.02$, for values of λ in the interval $\lambda \in [0.01, 0.15]$ with $\Delta\lambda = 0.01$, up to achieving the stationary state. The stationary state is reached when the time evolution of r (2) ends up in a constant vale. At this point, we measure the microscopic patterns of synchronization as described below.

The degree of synchrony between two connected nodes i and j is measured by quantifying the phase coherence[9,10] as follows:

$$C_{ij} = \lim_{T \to \infty} A_{ij} \left| \frac{1}{T} \int_{\tau}^{\tau+T} e^{i[\theta_i(t) - \theta_j(t)]} \, dt \right|. \quad (3)$$

Each of the values $\{C_{ij}\}$ are bounded in the interval [0,1], being $C_{ij} = 1$ when i and j are fully synchronized and $C_{ij} = 0$ when these nodes are dynamically uncorrelated or physically disconnected. Note that for a correct computation of the matrix **C** the averaging time T should be taken large enough (in our computations $T = 400$) to obtain reliable measures of the degree of coherence between each pair of nodes. Once the degree of synchronization between the nodes is measured, we filter the matrix **C** to construct a filtered matrix **F** whose elements are either $F_{ij} = 1$ if i and j are considered as synchronized or $F_{ij} = 0$ otherwise. To unveil what links are regarded as synchronized we compute the fraction of synchronized links as

$$r_{\text{link}} = \frac{1}{2L} \sum_{i,j} C_{ij}, \quad (4)$$

where L is the total number of links of the network ($L = \sum_{i,j=1}^{N} A_{ij}/2$). Therefore, one would expect that $2L \cdot r_{\text{link}}$ elements of the matrix F have $F_{ij} = 1$, while for the remaining elements $F_{ij} = 0$. The former elements correspond to the $2L \cdot r_{\text{link}}$ links with the largest values of C_{ij}. The matrix F

defines a new network, composed of those synchronized links. This new network is, in general, composed of several connected components being each of them a subgraph of the original network substrate. Thus, by means of the procedure described above we can describe these synchronized subgraphs (or clusters) for each value of λ. This description includes the number of synchronized clusters that coexist simultaneously in the system as well as their sizes, as given by their number of nodes and links, respectively.

III. RESULTS

For each topology, ER and SF, we have solved numerically the system of equations (1) for different values of the coupling constant λ in order to follow the evolution of the synchronized clusters. This enables to monitor the coalescence of pairs of synchronized oscillators as a function of λ. In this section, we will show that the microscopic path to synchronization is indeed different for both classes of networks. These differences in the behavior can be traced back to the growth of the largest cluster (or subgraph) of synchronized nodes, also known as giant synchronized component (GSC), as a function of λ. It turns out that for degree-homogeneous ER networks, many different clusters of synchronized pairs of oscillators merge together to form a macroscopic GSC when the coupling is increased. The union of many small clusters leads to a giant component of synchronized pairs that is almost of the size of the system (N) once the incoherent state destabilizes. The case is remarkably different for SF networks. In this case, the GSC grows gradually, and synchronized oscillators are incorporated to it in an almost sequential way as λ is increased.

In Fig. 1, we show the probability distribution of the size of the GSC, $P(N^{\text{sync}})$, for several values of the coupling strength λ for both ER and SF networks. The evolution of the distributions with λ for ER networks reveals the transition occurring when different synchronized clusters merge together to form a single GSC of macroscopic size. The transition occurs between $\lambda = 0.02$ and 0.04, and it is mediated by the nearly flat distribution shown for $\lambda = 0.03$. On the other hand, in SF networks, the distributions do not present this transition, and for all values of λ, $P(N^{\text{sync}})$ is clearly peaked and has a meaningful mean value for the average size of the GSC. Therefore, these distinct behaviors are already indicating that the path toward full synchronization depends on the heterogeneity of the degree distribution.

We also performed numerical experiments of adiabatic continuation in λ. For a given λ, we drive the system to its stationary state and induce a small perturbation of the coupling strength by incrementing it to $\lambda + \delta\lambda$ (with $\delta\lambda = 0.01$). Then, we record the changes in the size of the GSC, i.e., the number of new nodes that are incorporated into the GSC. This continuation allows us to obtain a more detailed picture of the evolution of the size of the GSC by monitoring its growth at the level of individual nodes incorporated and only those synchronized links between them. In this way, we count how many clusters of new nodes and synchronized links are present and finally compute the size of the GSC at the new λ value.
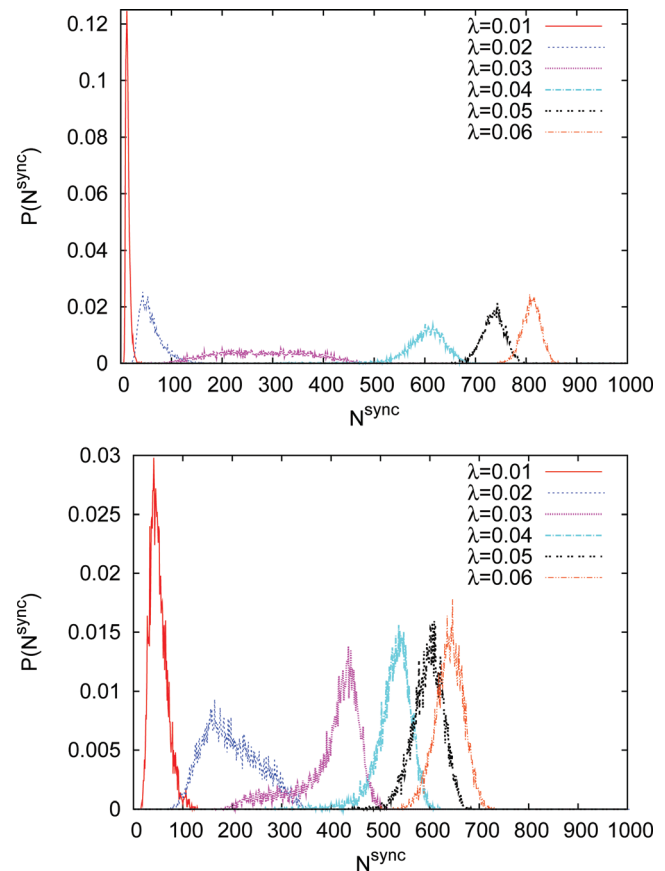

FIG. 1. (Color online) Size of the giant synchronized component. We plot here the probability of finding a giant synchronized component of a given size, N^{sync}, for different values of the coupling strength λ. The upper and bottom figures correspond to ER and SF networks, respectively. $N = 1000$ in both cases. The results for every value of λ are obtained using a sample of 10^4 different realizations. While for ER networks there is a clear gap in $P(N^{\text{sync}})$, SF networks show a gradual shift to the right without significant jumps in $P(N^{\text{sync}})$ as λ is increased.

In Fig. 2, we plot the function $N^{\text{sync}}(\lambda + \delta\lambda) = f[N^{\text{sync}}(\lambda)]$ obtained by performing the adiabatic continuation for several values of λ from 0.01 to 0.15. Every single numerical experiment is represented by a dot in the maps of Fig. 2 so that, after an extensive study (10^4 adiabatic continuations for each value of λ), we can observe the trends of the functions $f(x)$ of the maps corresponding to SF and ER topologies. The map obtained for ER networks confirms that when making a small change of the coupling around $\lambda = 0.02$, the GSC suddenly jumps from sizes of $N^{\text{sync}} \sim 10^2$ to $N^{\text{sync}} \sim 6 \times 10^2$ (recall that our simulations are done on top of networks of size $N = 10^3$). On the other hand, for SF networks the map does not present such dramatic changes for all the range of λ values explored. The color of the dots in both maps reveals that the size of the GSC of ER networks is $N^{\text{sync}} \sim N$ for low values of λ (for which the global degree of synchronization is still low[9,10]) while in SF networks such sizes proportional to N are only reached for large values of λ (in which a large global degree of synchrony is also observed[9,10]).

We have also explored the evolution of the number of links of the GSC. First, in Fig. 3, we have plotted the probability distribution of the number of synchronized links in the GSC for several values of λ. In the case of ER networks, we
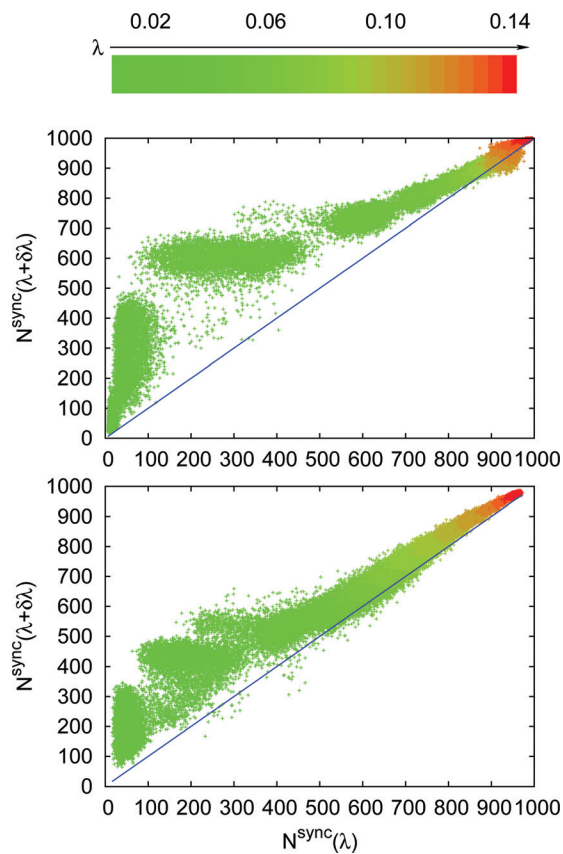
FIG. 2. (Color online) Evolution of the size of the *GSC* when increasing the coupling strength in ER (top) and SF (bottom) networks. To capture the growth of the *GSC* size as the coupling strength is increased from λ to $\lambda + \delta\lambda$ (with $\delta\lambda = 0.01$), we plot the function $N^{sync}(\lambda + \delta\lambda) = f[N^{sync}(\lambda)]$. A total number of 10^4 numerical continuations have been carried for every value of $\lambda \, \varepsilon \, [0.01, 0.14]$. The color of the dots denotes the corresponding value of λ as shown in the color bar.
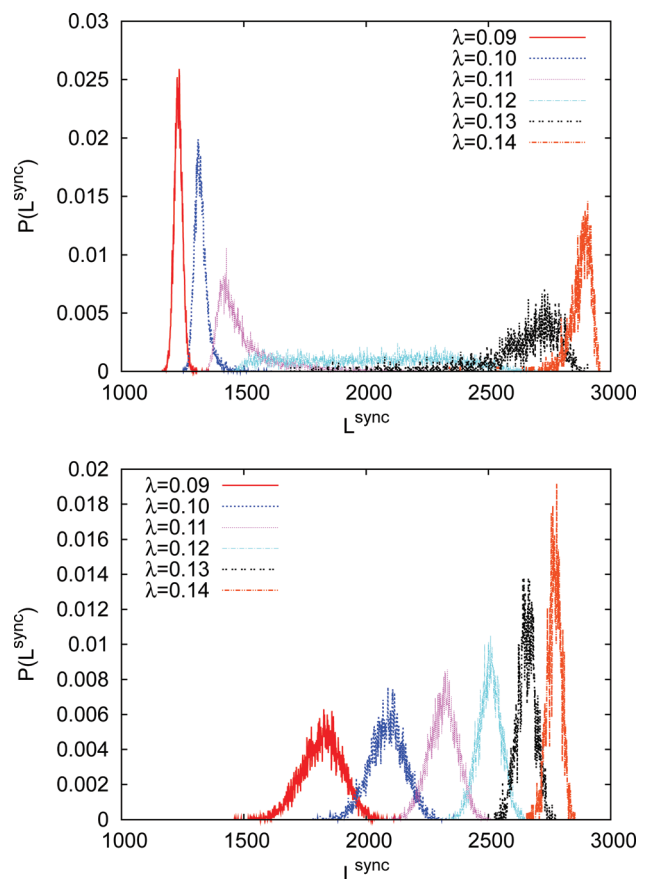

FIG. 3. (Color online) Number of synchronized links in the giant synchronized component. We plot the probability of finding a giant synchronized component with a given number of links, L^{sync}, for different values of the coupling strength λ. The upper and bottom figures correspond to ER and SF networks, respectively. The distributions are obtained as in Fig. 1.

observe a region of the coupling strength, around $\lambda = 0.12$, with a nearly flat distribution, thus signaling again dramatic changes in the structure of the *GSC* when the coupling is increased in this parametric region. At variance with Fig. 1, where the same phenomenology was observed, this flat distribution does not correspond to a growth of the *GSC*, but points out a fast addition of links connecting nodes that already belong to the *GSC* (those that joined it at lower values of λ). Therefore, in this region of λ, the synchronized links added do not contribute to the growth of the *GSC* (it is already of order *N*), but to the decrease of the average path length between its nodes (see below). On the other hand, the SF topology shows a smooth evolution of the probability distributions and their corresponding mean values, pointing out a gradual addition of synchronized links as λ increases.

By using again the adiabatic continuation in λ, we can carefully check how the addition of links to the *GSC* takes place. We performed 5×10^3 numerical experiments of adiabatic continuation from $\lambda = 0.01$ to $\lambda = 0.14$ with $\Delta\lambda = 0.01$. In Fig. 4, we show the scatter plots for the number of links, $L^{sync}(\lambda + \delta\lambda) = g[L^{sync}(\lambda)]$, for both SF and ER networks. From this figure, it becomes evident that the addition of links into the *GSC* in SF networks proceeds in a smooth way similarly to its growth in size. On the other hand, for ER networks, we find evidences of two sudden jumps during the adi-

abatic continuation. In particular, for values of the coupling in the region $\lambda \in [0.1, 0.12]$, for which the size of the *GSC* is of the order of the size of the substrate ER network, we observed a sudden addition of links that connect nodes already belonging to the *GSC*.

Finally, we analyzed the evolution of the average path length (*APL*) of the *GSC*, $\langle l \rangle^{sync}$, when passing from local to global synchronization. The idea here is to provide another indication of the structural differences in the *GSC* for the different classes of networks, when changing the coupling between oscillators. In Fig. 5, we show this variation by plotting the map $\langle l \rangle^{sync}(\lambda + \delta \, \lambda) = h[\langle l \rangle^{sync} (\lambda)]$ obtained after 10^4 realizations for each value of λ for both ER and SF networks. In both cases, the *APL* is normalized to the *APL* of the corresponding substrate network. From Fig. 5, it is clear that the *GSC* of ER networks reaches *APL* values remarkably larger than those obtained in SF networks along the synchronization path. Moreover, in ER networks and for large values of λ we observe a fast collapse to the value of the *APL* of the substrate network from configurations that are twice longer than the substrate. This sudden collapse occurs in the region of λ where the massive addition of links was observed in Fig. 4. On the other hand, in SF networks the transition from large values of the *APL* to the length of the substrate
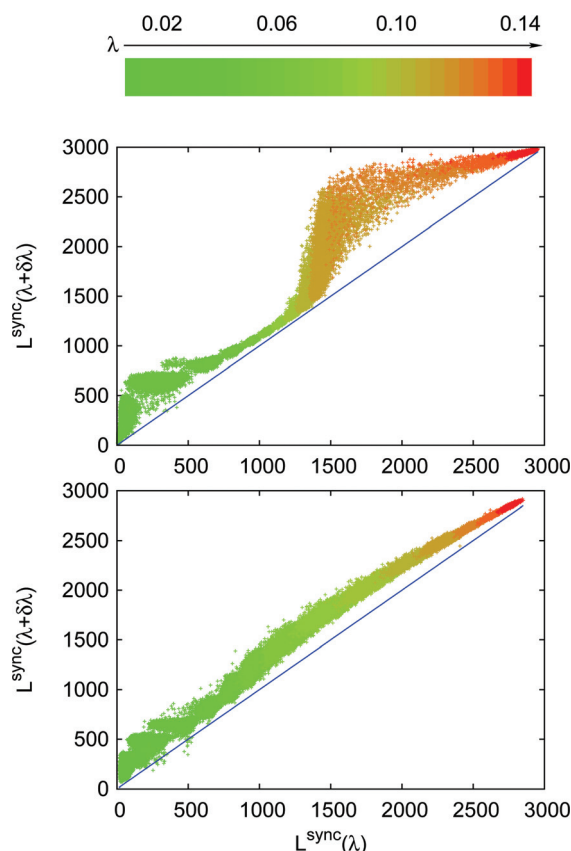
FIG. 4. (Color online) Number of synchronized links, L^{sync}, after increasing the coupling. Same philosophy as Fig. 2: We construct the map $L^{\text{sync}}(\lambda + \delta\lambda) = g[L^{\text{sync}}(\lambda)]$ by following the evolution of the synchronized *GSC* as the coupling λ is increased from 0.01 to 0.15. The evolution for the ER network (top) shows two big jumps in the number of links incorporated into the *GSC* in contrast with the continuous shape of $g(x)$ for the SF topology (bottom). Both panels show a number of 10^4 numerical continuations.

FIG. 5. (Color online) Evolution of the average path length of the *GSC* along the synchronization path. We show the change in the *APL* of the *GSC* of ER (top) and SF (bottom) networks when passing from λ to $\lambda + \delta\lambda$ with $\delta\lambda = 0.01$. In both panels, we plot the relation $\langle l \rangle^{\text{sync}}(\lambda + \delta\lambda) = h[\langle l \rangle^{\text{sync}}(\lambda)]$ observed in 10^4 numerical continuation along the range $\lambda\,\varepsilon\,[0.01, 0.14]$. As denoted by the dotted *line* in the top panel, a sudden decrease of the *APL* in the *GSC* of ER networks occurs at $\lambda \simeq 0.12$ due to the fast addition of links into the *GSC*. Such a dramatic change is not observed for SF networks, and the APL gradually decreases as shown by the dotted line.

networks takes place smoothly since link addition is also a sequential process bringing new nodes to the *GSC*.

IV. CONCLUSIONS

Summarizing, we have explored numerically the synchronization of Kuramoto oscillators in complex topologies as the coupling strength is increased driving the system's dynamics to the fully synchronized state. By carefully characterizing the way in which the size and composition of the *GSC* changes, we have explored the paths toward synchronization in homogeneous and heterogeneous networks. All the extensive simulations performed on the two topologies, ER and SF, clearly indicate that the evolution of the *GSC* is different in both classes of networks.

We have presented raw data from the numerical experiments without any type of processing, averaging or any other coarse-graining of the information. Therefore, our results put in evidence the statistical analysis performed by the authors of Ref. 11 and the claimed coincidence of the scaling exponents there derived. The conclusion is then that the suitability of such approaches has to be confirmed first and therefore cannot be used as the base of the claim raised to invalidate our previous findings, which are doubtlessly corroborated here. As any theory intended to explain the results of a nu-
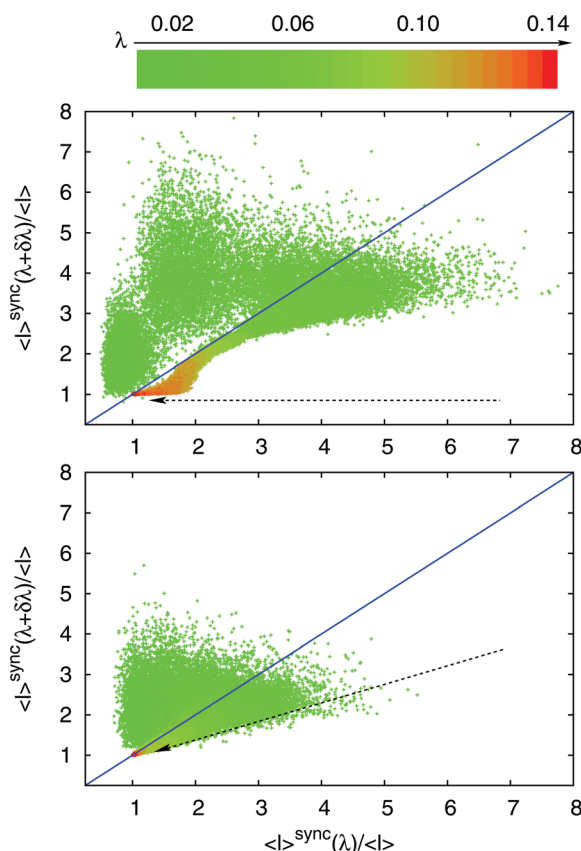
merical experiment, when numerics and theory do not agree, the theory must be revised.

ACKNOWLEDGMENTS

[1]A. T. Winfree, *The Geometry of Biological Time* (Springer-Verlag, New York, 1990).
[2]S. H. Strogatz, *Sync: The Emerging Science of Spontaneous Order* (Hyperion, New York, 2003).
[3]S. C. Manrubia, A. S. Mikhailov, and D. H. Zanette, *Emergence of Dynamical Order. Synchronization Phenomena in Complex Systems* (World Scientific, Singapore, 2004).
[4]S. H. Strogatz, Nature **410**, 268 (2001).
[5]R. Albert and A.-L. Barabasi, Rev. Mod. Phys. **74**, 47 (2002).
[6]M. E. J. Newman, SIAM Rev. **45**, 167 (2003).
[7]S. Boccaletti, V. Latora, Y. Moreno, M. Chavez, and D.-U. Hwang, Phys. Rep. **424**, 175 (2006).
[8]A. Arenas, A. Díaz-Guilera, J. Kurths, Y. Moreno, and C. Zhou, Phys. Rep. **469**, 93 (2008).

[9]J. Gómez-Gardeñes, Y. Moreno, and A. Arenas, Phys. Rev. Lett. **98**, 034101 (2007)

[10]J. Gómez-Gardeñes, Y. Moreno, and A. Arenas, Phys. Rev. E **75**, 066106 (2007).

[11]Y. Kim, Y. Ko, and S.-H. Yook, Phys. Rev. E **81**, 011139 (2010).

[12]Y. Moreno and A. F. Pacheco, EPL **68**, 603 (2004).

[13]T. Ichinomiya, Phys. Rev. E **70**, 026116 (2004).

[14]E. Oh, K. Rho, H. Hong, and B. Kahng, Phys. Rev. E **72**, 047101 (2005).

[15]D.-S. Lee, Phys. Rev. E **72**, 026208 (2005).

[16]J. G. Restrepo, E. Ott, and B. R. Hunt, Chaos **16**, 015107 (2006).

[17]C. Zhou and J. Kurths, Chaos **16**, 015104 (2006).

[18]Y.-Ch. Hung, Y.-T. Huang, M.-Ch. Ho, and Ch.-K. Hu, Phys. Rev. E **77**, 016202 (2008).

[19]T. Pereira, Phys. Rev. E **82**, 036201 (2010).

[20]M. Chen, Y. Shang, Y. Zou, and J. Kurths, Phys. Rev. E **77**, 027101 (2008).

[21]X. Wang, L. Huang, Sh. Guan, Y.-Ch. Lai, and Ch. H. Lai, Chaos **18**, 037117 (2008).

[22]J. Gómez-Gardeñes and Y. Moreno, Int. J. Bifurcation Chaos **17**, 2501 (2007).

[23]M. Brede, Eur. Phys. J. B **62**, 87 (2008).

[24]A. Arenas, A. Diaz-Guilera, and C. J. Perez-Vicente, Phys. Rev. Lett. **96**, 114102 (2006).

[25]A. Díaz-Guilera, J. Gómez-Gardeñes, Y. Moreno, and M. Nekovee, Int. J. Bifurcation Chaos **19**, 687 (2009).

[26]W.-X. Wang, L. Huang, Y.-Ch. Lai, and G. Chen, Chaos **19**, 013134 (2009).

[27]K. A. Schindler, S. Bialonski, M.-Th. Horstmann, Ch. E. Elger, and K. Lehnertz, Chaos **18**, 033119 (2008).

[28]E. Fuchs, A. Ayali, E. Ben-Jacob, and S. Boccaletti, Phys. Biol. **6**, 036018 (2009).

[29]C. S. Zhou, L. Zemanová, G. Zamora-López, C. C. Hilgetag, and J. Kurths, New J. Phys. **9**, 178 (2007).

[30]J. Gómez-Gardeñes, G. Zamora-López, Y. Moreno, and A. Arenas, PLoS ONE **5**, e12313 (2010).

[31]Y. Kuramoto, Prog. Theor. Phys. **79**, 223 (1984).

[32]S.H. Strogatz, Physica D **143**, 1 (2000).

[33]J. A. Acebron, L. L. Bonilla, C. J. Perez Vicente, F. Ritort, and R. Spigler, Rev. Mod. Phys. **77**, 137 (2005).

[34]J. Gómez-Gardeñes and Y. Moreno, Phys. Rev. E **73**, 056124 (2006).